NUCL SCI TECH (2017) 28:123
DOI 10.1007/s41365-017-0281-0

# Crystal structure determination of a chimeric FabF by XRD

**Ke Li[1,2] · Li Li[2] · Ye-Chun Xu[2]**

Received: 15 November 2016 / Revised: 22 December 2016 / Accepted: 30 December 2016 / Published online: 5 August 2017


**Abstract** Beta-ketoacyl-acyl-carrier-protein synthase II, an important enzyme in biosynthesis of bacterial fatty acid, is an attractive target in antibacterial drug design. Platensimycin (PTM), produced by *Streptomyces platensis*, has a strong, broad-spectrum Gram-positive antibacterial activity by selectively targeting to FabF but exhibits no inhibition to the FabF from *Streptomyces platensis* (spFabF). To study the self-resistance mechanism within the PTM-producing strain and provide hint for development of novel antibiotics, it is imperative to solve the structure of spFabF and elucidate the difference between spFabF and other FabFs which are not resistant to PTM. To this end, we constructed four chimeric FabFs based on the sequence of spFabF and its homologous protein after the expression of wide-type spFabF was failed. The crystal structure of one chimera, $js_{200}$FabF, of 91.2% sequence identity to spFabF, was solved. A structure comparison of $js_{200}$FabF with a PTM-bound FabF suggested that three loops nearby the catalytic site might play key roles in preventing the binding of PTM to spFabF. The results provide an encouraging basis for further studies on the self-resistance mechanism and structure-based design of novel antibiotics targeting FabFs.

**Keywords** FabF · Chimera · X-ray diffraction · Crystal structure determination

## 1 Introduction

Fatty acids are essential building blocks used in assembly of many important bacterial components such as phospholipids, lipoproteins and lipopolysaccharides. Fatty acid synthase (FAS) plays crucial roles in biosynthesis of bacterial fatty acids [1–5]. While type I FASs are found in animals, fungi and lower eukaryotes, type II enzymes are found in prokaryotes, plastids and mitochondria. Both types are attractive targets for antibiotics [6]. Beta-ketoacyl-acyl-carrier-protein synthases (KAS) are important members of the FAS(II) family, including KAS I (FabB), KAS II (FabF) and KAS III (FabH). FabH catalyzes the initiation of fatty acid elongation by condensing malonyl-ACP with acetyl-CoA. FabB and FabF, which catalyze acyl-ACP reactions with malonyl-ACP, can produce long-chain acyl-ACPs [7]. FabFs catalyze unique condensation reactions that are essential steps for chain elongation in fatty acid biosynthesis, hence showing the importance of antibacterial drug discovery.

Platensimycin (PTM), produced by *Streptomyces platensis* (*S. platensis*), has potent, broad-spectrum Gram-positive antibacterial activity and exhibits no cross-resistance to other key antibiotic-resistant bacteria such as methicillin-resistant *Staphylococcus aureus* (*S. aureus*), vancomycin-resistant *Enterococci*, vancomycin-intermediate *S. aureus*, and linezolid-resistant and macrolide-

This work was supported by the National Natural Science Foundation of China (Nos. 81502987 and 81422047).

✉ Ye-Chun Xu
ycxu@simm.ac.cn

[1] College of Science, Shanghai University, 99 Shangda Road, Shanghai 200444, China

[2] CAS Key Laboratory of Receptor Research, Drug Discovery and Design Center, Shanghai Institute of Materia Medica, Chinese Academy of Sciences (CAS), Shanghai 201203, China

resistant pathogens [8]. The antibacterial effect of PTM was achieved by selectively targeting to FabF/B in the synthetic pathway of fatty acids [8–10]. Recently, it was reported that FabF from the PTM-producing *S. platensis* resisted PTM [11], but the underlying molecular mechanism is not clear yet. In this work, aimed at providing structural interpretation for the difference between the FabF from *S. platensis* (spFabF) and other FabFs which are susceptible to PTM, we tried to solve the crystal structure of spFabF. A chimeric protein design strategy was applied to obtain the soluble protein of spFabF. X-ray diffraction of multiple crystals of the chimeric FabF, namely $js_{200}$FabF, was performed on Beamline BL17U1 of Shanghai Synchrotron Radiation Facility (SSRF), with the resolution of 3.15 Å. The structural difference between $js_{200}$FabF and the PTM-bound FabF from *E. coli* (ecFabF) was discussed for the resistance of spFabF to PTM.

## 2 Experimental section

### 2.1 Protein expression and purification

The wide type of full-length spFabF with fusion proteins including TRX, MBP and GST, and four chimeras as well constructed on the basis of spFabF and its homologous genes *Streptomyces albus* J1074 FabF (saFabF) (Fig. 1) were subcloned into the vector pET-28a with a TEV protease cleavage site following a six-His tag added at the N terminus. Restriction sites BamHI and XhoI were used. The DNA sequence of the wide-type spFabF and saFabF were synthesized by the company of Generay Biotech (*Shanghai*). The primers used for gene amplification are listed in Table 1.

The recombinant plasmids were transformed into *E. coli* BL21 (DE3) cells [12]. Cells harboring this expression plasmid were grown in LB containing 50 μg/mL kanamycin to the mid-log phase at 37 °C. Subsequently, the culture was induced by 0.1 mM isopropyl β-D-1-thiogalactopyranoside (IPTG) and incubated for 14–16 h at 16 °C. The cell pellets were harvested, re-suspended and lysed with the buffer consisting of 20 mM Tris pH 8.0, 10% (v/v) glycerol, 500 mM NaCl, 5 mM BME (β-mercaptoethanol) and 20 mM imidazole. The lysate was centrifuged. The supernatant was loaded on a 10-ml Ni–NTA Sepharose column (*GE Healthcare*). The column was washed with buffer A containing 20 mM Tris pH 8.0, 10% (v/v) glycerol, 500 mM NaCl, 5 mM BME and 80 mM imidazole, until no further protein was detected by the Bio-Rad protein-assay kit, and then eluted with buffer B containing 20 mM Tris pH 8.0, 10% (v/v) glycerol, 500 mM NaCl, 5 mM BME and 250 mM imidazole. The eluted fraction was concentrated and further loaded on the Superdex$^{TM}$ 200 20/300 GL column (*GE Healthcare*) which is equilibrated in a gel filtration buffer consisting of 20 mM Tris pH 8.0, 100 mM NaCl, 10% (v/v) glycerol, 1 mM DL-Dithiothreitol (DTT). The eluted protein was concentrated to 10 mg/ml for crystallization.

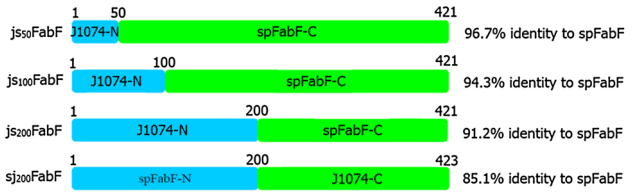


**Fig. 1** (Color online) Scheme of four designed chimeric FabFs. *Cyan* and *green* regions represent the sequence of saFabF and spFabF, respectively. The sequence identities of the chimeric FabFs to sbFabF were shown in the right. Taking $js_{50}$FabF as an example, the first 50 amino acids are from the N-terminal 50 residues of saFabF, the last 371 amino acids are from the C-terminal 371 residues of spFabF, and the sequence identity of $js_{50}$FabF to spFabF is 96.7%

### 2.2 Protein crystallization

Screening of the initial crystallization conditions was carried out using the sparse matrix approach with a series of kits including Index, Crystal Screen, Crystal Screen 2, PEG/Ion, PEG/Ion 2, SaltRx, SaltRx 2, PEGRx, PEGRx 2 (*Hampton Research*) and Wiz1–4 (*Emerald BioSystems*). Crystallization was performed at 4 and 20 °C using a sitting-drop vapor-diffusion method by mixing equal volumes of the protein solution (1 μL) and reservoir solution (1 μL). Once the crystal was grown, the vapor-diffusion method in hanging drops was utilized to optimize the condition. The perfluoropolyether PFO-X175/08 (Hampton Research) [13] was used as a cryoprotectant for all of the crystals. The crystals were picked up with cryo-loops and flash-frozen in liquid nitrogen.

### 2.3 Data collection and processing (Table 2)

X-ray diffraction data were collected at 100 K on Beamline BL17U1 at SSRF [14], with the wavelength of 0.97923 Å and the crystal-to-detector distance of 250 mm. A total of 360 frames were collected with 0.5° oscillation and 1 s exposure time per frame. The data were processed with the HKL-2000 software package [15]. Molecular replacement was performed with Phaser [16] using the structure of *Thermus thermophilus* FabF (PDB code 1J3N) [17] as a search model. The structure was refined with the program of Phenix [18]. Using the program of Coot [19], water molecules were fitted into to the initial $F_o - F_c$ map.

**Table 1** Primers used for molecular cloning

| | | |
|---|---|---|
| $js_{50}$FabF primer | N-J50 forward primer | CGCGGATCCATGAGCCCGACCAATCGTACC |
| | N-J50 reverse primer | CTGCCTGTGCTGCAATACGAACCGGCAGGTCCGCATAACGTTC |
| | C-S50 forward primer | GAACGTTATGCGGACCTGCCGGTTCGTATTGCAGCACAGGCAG |
| | C-S50 reverse primer | CCGCTCGAGTTAAACGGTACGAAATGCCAG |
| $js_{100}$FabF primer | N-J100 forward primer | N-J50 forward primer |
| | N-J100 reverse primer | CACCAATACCGCTTGCAATAACTGTTCCCAGACGTTCCGGGCT |
| | C-S100 forward primer | AGCCCGGAACGTCTGGGAACAGTTATTGCAAGCGGTATTGGTG |
| | C-S100 reverse primer | C-S50 reverse primer |
| $js_{200}$FabF primer | N-J200 forward primer | N-J50 forward primer |
| | N-J200 reverse primer | CTGCAATCGGCAGCGGATGAATTGCTGCTTCCGTGCCACCTGC |
| | C-S200 forward primer | GCAGGTGGCACGGAAGCAGCAATTCATCCGCTGCCGATTGCAG |
| | C-S200 reverse primer | C-S50 reverse primer |
| $sj_{200}$FabF primer | N-S200 forward primer | CGCGGATCCATGAATGCAACCAATCGTAC |
| | N-S200 reverse primer | CAACAACCGGCAGCGGATGAATTGCTGCTTCAGTACCACCTGC |
| | C-J200 forward primer | GCAGGTGGTACTGAAGCAGCAATTCATCCGCTGCCGGTTGTTG |
| | C-J200 reverse primer | CCGCTCGAGTTAAACGGTACGAAATGCCAG |

**Table 2** Data collection and refinement statistics for the crystal structure of $js_{200}$FabF

| | |
|---|---|
| Data collection | |
| Wavelength (Å) | 0.97923 |
| Temperature (K) | 100 |
| Resolution (Å) | 50–3.15 (3.26–3.15) |
| Total no. of reflections | 1,326,684 |
| No. of unique reflections | 24,808 |
| Redundancy | 10.5 |
| Completeness (%) | 94.4 |
| Mean $I/\sigma$ | 12.7 |
| $R_{merge}$ | 0.174 |
| Space group | $P3_221$ |
| Unit cell parameters | |
| $a$ (Å) | 160.27 |
| $b$ (Å) | 160.27 |
| $c$ (Å) | 95.57 |
| $\alpha, \beta, \gamma$ (°) | 90, 90, 120 |
| Refinement | |
| $R_{work}$ | 0.1958 |
| $R_{free}$ | 0.2790 |
| R.m.s.d from ideality | |
| Bonds (Å) | 0.013 |
| Angles (°) | 1.476 |
| Ramachandran plot | |
| Allowed regions (%) | 95.1 |
| Disallowed regions (%) | 4.9 |

## 3 Results and discussion

### 3.1 Design of chimeric FabFs

The expression and purification of the wide-type spFabF with different fusion proteins in *E. coli*, as described in Sect. 2, led to the aggregates of the protein. A chimeric protein design strategy was subsequently applied. Sequence alignment suggested that saFabF might be of the highest sequence identity to spFabF (76.4%). The chimeric FabFs were thus constructed with the combination of spFabF and saFabF. In general, the N-terminal region of saFabF was used in the chimeric proteins because that its sequence was more identical than the C-terminal to spFabF. The first 200 amino acid residues of saFabF showed 81.5% sequence identity to the corresponding residues of spFabF. Four chimeras, namely $js_{50}$FabF, $js_{100}$FabF, $js_{200}$FabF and $sj_{200}$FabF, were designed (Fig. 1). Taking $js_{200}$FabF as an example, the first 200 amino residues from the N-terminal of saFabF and the last 200 residues from the C-terminal of spFabF were combined (Fig. 1). The resulted $js_{200}$FabF had 91.2% sequence identity to the wide type of spFabF.

The chimeric proteins were also expressed in *E. coli*. The overexpressed proteins were purified by a Ni–NTA affinity chromatography together with a gel filtration chromatography to obtain the homogeneous soluble proteins. The gel filtration chromatographic experiment suggested that only $js_{200}$FabF might have proteins of low

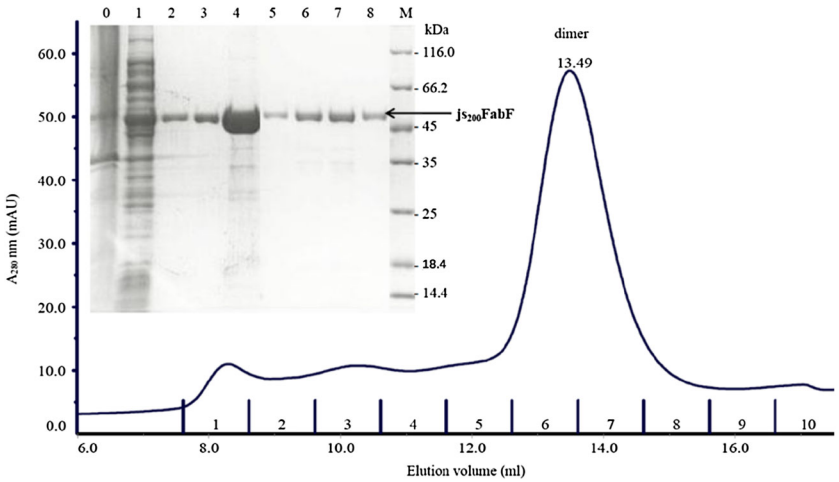


**Fig. 2** Characterization of $js_{200}$FabF by the analytical size exclusion chromatography and SDS-PAGE. $js_{200}$FabF was eluted with a peak at 13.49 mL of the Superdex$^{TM}$ 200 20/300 GL column. In the SDS-PAGE, Lanes 0–4 represent the pellet resulted from the cell lysate, the flow-through from the NTA affinity column, the elute from the NTA affinity column with buffer A (containing 80 mM imidazole), the elute from the NTA affinity column with buffer B (containing 250 mM imidazole) and the concentrated sample used for the size exclusion chromatography, respectively. Lane M represents molecular weight markers labeled in kDa. Lanes 5–8 are corresponding to the fractions 5–8 from the size exclusion chromatography

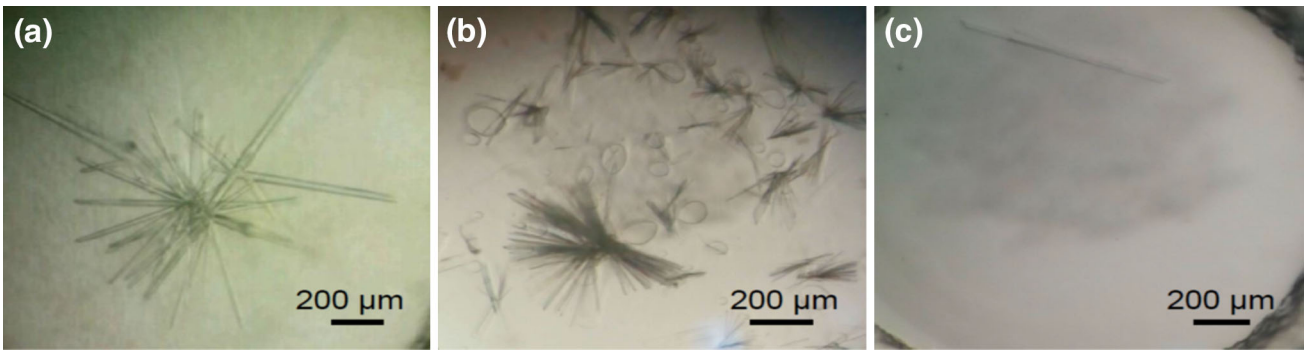


**Fig. 3** (Color online) Crystals of $js_{200}$FabF grown with a reservoir containing 0.1 M sodium chloride, 0.1 M bicine pH 9.0, 20% (v/v) PEG MME 550 (**a**); 0.1 M HEPES pH 7.5, 12% PEG 3350 (**b**); and 0.1 M Bis–Tris pH 5.5, 25% PEG 3350, 0.2 M ammonium sulfate (**c**), respectively

molecular weight, while the other three were aggregates. A further characterization of the low molecular weight samples with the analytical size exclusion chromatography showed that a single peak eluting at about 13.49 mL, which is usually corresponding to a protein of molecular weight around 90 kDa (Fig. 2). It is thus conjectured that $js_{200}$FabF was a comparatively stable dimer in solution. The SDS-PAGE showed that the proteins are quite pure (purity over 95%).

### 3.2 Screening of crystallization conditions for $js_{200}$FabF

After the pure and dimeric $js_{200}$FabF was concentrated to 10 mg/mL, a crystallization condition screening was carried out using multiple screening kits. Rod crystals of the protein were obtained under conditions containing salts (the majority) or PEGs (rare) as a precipitating agent. However, these crystals had the low-resolution diffraction properties. The crystals from the condition No. 46 of Crystal Screen 2 consisting of 0.1 M NaCl, 0.1 M bicine pH 9.0, 20% (v/v) PEG MME 550 (Fig. 3a) and the condition No. 30 of PEGRx consisting of 0.1 M HEPES pH 7.5, 12% PEG 3350 (Fig. 3b) were in bar shapes. The crystal with the best diffraction was obtained using a reservoir solution consisting of 0.1 M Bis–Tris pH 5.5, 25% PEG 3350, 0.2 M ammonium sulfate (Fig. 3c). The crystals grown at 4 °C often showed better diffraction quality than those grown at 20 °C. However, the crystal growth at 4 °C took about half a year before it was ready for XRD experiment. Besides, the six-His tag at the N-terminal of $js_{200}$FabF showed no apparent effects on crystallization and diffraction.

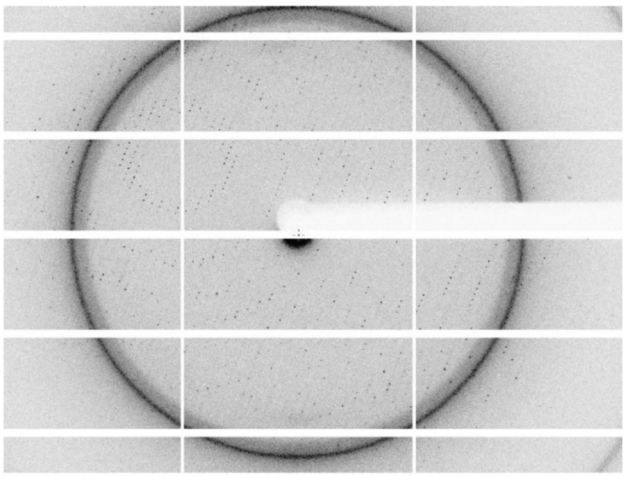

**Fig. 4** A typical XRD result of the $js_{200}$FabF crystal

### 3.3 Structure determination

Crystals of $js_{200}$FabF were flash-cooled in liquid nitrogen with a cryoprotectant and examined by XRD. An example of the XRD results is shown in Fig. 4. The data processing indicated that it belonged to the cubic space group $P3_221$, with unit cell parameters of $a = 160.27$ Å, $b = 160.27$ Å and $c = 95.57$ Å. The calculated Matthews coefficient ($V_M$) was 2.32 Å$^3$/Da with 47.01% solvent content, assuming the presence of six molecules in the asymmetric unit [20]. The structure of $js_{200}$FabF was finally solved with the best resolution of 3.15 Å.

PTM is a potent inhibitor of FabF from *E. coli* (ecFabF) and the crystal structures of the mutant ecFabF(C163Q and C163A) in complex with PTM are the only known structure of FabF bound with PTM [8, 21]. Although the sequence identity of $js_{200}$FabF to ecFabF was 39.8%, the superimposition of two

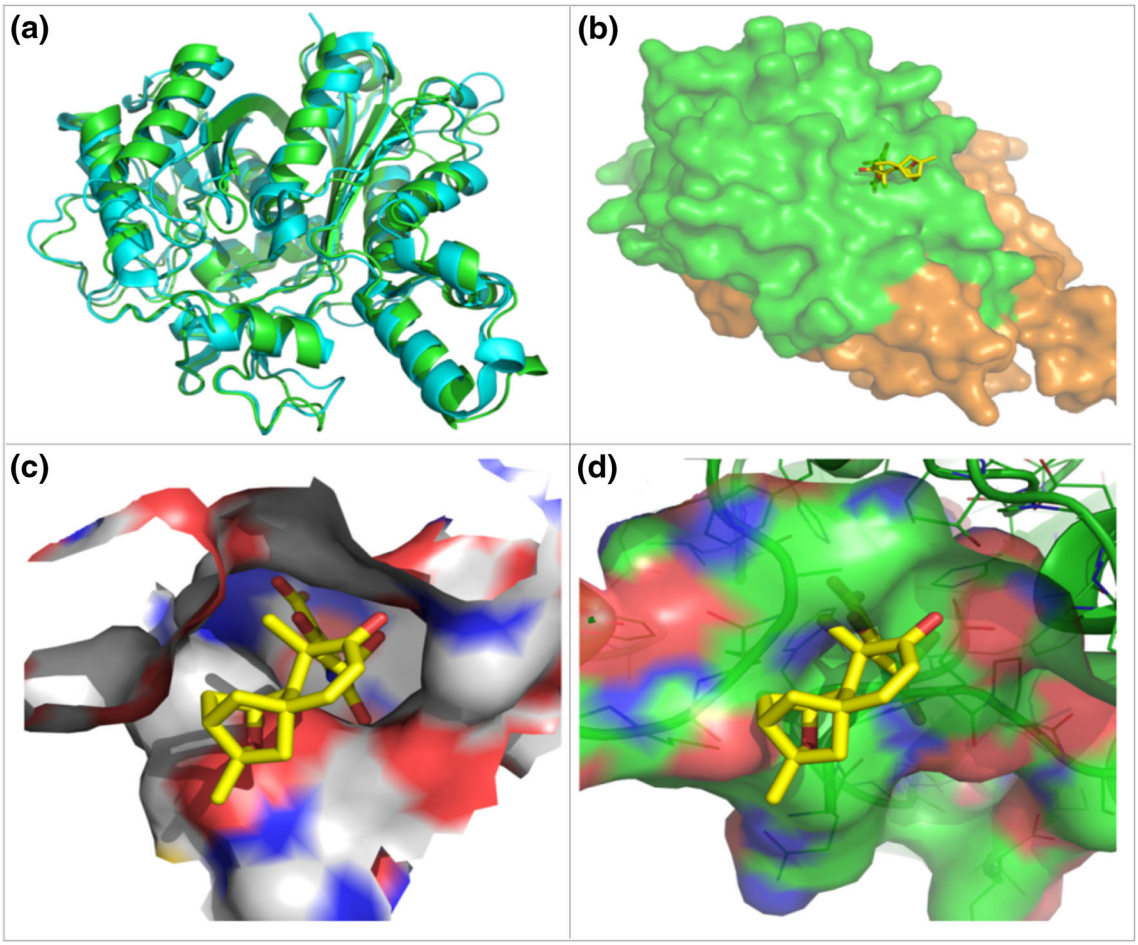


**Fig. 5** (Color online) Superimposition of $js_{200}$FabF with ecFabF. **a** Cartoon representation of $js_{200}$FabF (*green*) and ecFabF (*cyan*) (PDB code 2GFW). **b** Molecular surface of $js_{200}$FabF. *Orange* and *green* represent the first 200 and the last 221 residues of $js_{200}$FabF, respectively. The position of PTM shown in *yellow sticks* was taken from the superimposed ecFabF(C163Q) in complex with PTM. **c** Binding pocket of PTM in ecFabF(C163Q). **d** Overlap of the superimposed PTM with the assumed ligand binding pocket of PTM in $js_{200}$FabF

structures in Fig. 5a revealed that the topology of $js_{200}$FabF was similar to ecFabF. In addition, according to the complex structure of PTM bounded ecFabF(C163Q), the binding site for PTM in $js_{200}$FabF should be located at the C-terminal region, and the sequence was completely identical to the C-terminal of spFabF (Fig. 5b). This means that $js_{200}$FabF can be regarded as spFabF in studying the PTM binding to spFabF. Exploring the binding pocket of PTM in ecFabF(C163Q) and of spFabF, we found that the three loops (residues 211–215, 277–281 and 407–411) adopted different conformations as compared with them in ecFabF(C163Q), resulting that the assumed ligand binding pocket of PTM in spFabF was greatly occupied by these loop residues and the superimposed PTM had many bumping with the neighboring residues of spFabF (Fig. 5c, d). Therefore, the different conformations of three loops may account for the resistance of spFabF to PTM.

## 4 Conclusions

We constructed four chimeric FabFs based on spFabF from the PTM-producing *S. platensis* and its homologous protein in an attempt to solve the structure of spFabF and to interpret its resistance to PTM which is a potent and selective inhibitor of bacterial FabFs. One of the chimeras, $js_{200}$FabF, could be expressed in *E. coli* and purified with a pure and stable dimer protein for crystallization. The protein crystal best diffracted to 3.15 Å was grown in the condition containing 0.1 M Bis–Tris pH 5.5, 25% PEG 3350 and 0.2 M ammonium sulfate. The solved structure shown that $js_{200}$FabF has a similar topology to other FabFs such as ecFabF. As compared to the structure of ecFabF in complex with PTM, three loops nearby the catalytic site change their conformations, reduce the volume of the assumed ligand binding pocket and thus prevent the binding of PTM to spFabF. However, in view of the low resolution of the present structure, the high flexibility of loops and the fact that $js_{200}$FabF has 91.2% sequence identity to sbFabF, further efforts will be made to determine the high-resolution structure of sbFabF and to use other methodologies to study the effect of loop dynamics on the binding of PTM to FabFs.

**Acknowledgements** We are grateful to the staff at Beamline BL17U1 of Shanghai Synchrotron Radiation Facility (SSRF) for excellent technical assistance during data collection.

## References

1. J.W. Campbell, J.E. Cronan, Bacterial fatty acid biosynthesis: targets for antibacterial drug discovery. Annu. Rev. Microbiol. **55**, 305–332 (2001). doi:10.1146/annurev.micro.55.1.305
2. Y.M. Zhang, H. Marrakchi, S.W. White et al., The application of computational methods to explore the diversity and structure of bacterial fatty acid synthase. J. Lipid Res. **44**, 1–10 (2003). doi:10.1194/jlr.R200016-JLR200
3. R.J. Heath, C.O. Rock, Fatty acid biosynthesis as a target for novel antibacterials. Curr. Opin. Investig. Drugs **5**, 146–153 (2004)
4. S. Smith, A. Witkowski, A.K. Joshi, Structural and functional organization of the animal fatty acid synthase. Prog. Lipid Res. **42**, 289–317 (2003). doi:10.1016/S0163-7827(02)00067-X
5. S.W. White, J. Zheng, Y.M. Zhang, The structural biology of type II fatty acid biosynthesis. Annu. Rev. Biochem. **74**, 791–831 (2005). doi:10.1146/annurev.biochem.74.082803.133524
6. C.E. Christensen, B.B. Kragelund, P.V. Wettstein-Knowles et al., Structure of the human β-ketoacyl [ACP] synthase from the mitochondrial type II fatty acid synthase. Protein Sci. **16**, 261–272 (2007). doi:10.1110/ps.062473707
7. X. Qiu, C.A. Janson, W.W. Smith et al., Refined structures of beta-ketoacyl-acyl carrier protein synthase III. J. Mol. Biol. **307**, 341–356 (2001). doi:10.1006/jmbi.2000.4457
8. J. Wang, S.M. Soisson, K. Young et al., Platensimycin is a selective FabF inhibitor with potent antibiotic properties. Nature **441**, 358–361 (2006). doi:10.1038/nature04784
9. S.B. Singh, H. Jayasuriya, J.G. Ondeyka et al., Isolation, structure, and absolute stereochemistry of platensimycin, a broad spectrum antibiotic discovered using an antisense differential sensitivity strategy. J. Am. Chem. Soc. **128**, 11916–11920 (2006). doi:10.1021/ja062232p
10. M. Wu, S.B. Singh, J. Wang et al., Antidiabetic and antisteatotic effects of the selective fatty acid synthase (FAS) inhibitor platensimycin in mouse models of diabetes. Proc. Natl. Acad. Sci. **108**, 5378–5383 (2011). doi:10.1073/pnas.1002588108
11. R. Peterson, T. Huang, J. Rudolf et al., Mechanisms of self-resistance in the platensimycin-and platencin-producing streptomyces platensis MA7327 and MA7339 strains. Chem. Biol. **21**, 389–397 (2014). doi:10.1016/j.chembiol.2014.01.005
12. Y.X. Chen, M.J. Li, F. Yu et al., Using Xe as a heavy atom for phase determination of protein trichosanthin structure. Nucl. Sci. Tech. **25**, 60–64 (2014). doi:10.13538/j.1001-8042/nst.25.030502
13. Y. Xu, M.J. Li, H. Greenblatt et al., Flexibility of the flap in the active site of BACE1 as revealed by crystal structures and molecular dynamics simulations. Acta Crystallogr. D **68**, 13–25 (2012). doi:10.1107/S0907444911047251
14. Q.S. Wang, F. Yu, S. Huang et al., The macromolecular crystallography beamline of SSRF. Nucl. Sci. Tech. **26**, 010102 (2015). doi:10.13538/j.1001-8042/nst.26.010102
15. Z. Otwinowski, W. Minor, Processing of X-ray diffraction data collected in oscillation mode. Methods Enzymol. **276**, 307–326 (1997). doi:10.1016/S0076-6879(97)76066-X
16. A.J. McCoy, R.W. Grosse-Kunstleve, P.D. Adams et al., Phaser crystallographic software. J. Appl. Cryst. **40**, 658–674 (2007). doi:10.1107/S0021889807021206
17. B. Bagautdinov, Y. Ukita, M. Miyano et al., Structure of 3-oxoacyl-(acyl-carrier protein) synthase II from Thermus thermophilus HB8. Acta Crystallogr. F **64**, 358–366 (2008). doi:10.1107/S1744309108010336
18. P.D. Adams, P.V. Afonine, G. Bunkoczi et al., PHENIX: a comprehensive python-based system for macromolecular structure solution. Acta Crystallogr. D **66**, 213–221 (2010). doi:10.1107/S0907444909052925
19. P. Emsley, K. Cowtan, Coot: model-building tools for molecular graphics. Acta Crystallogr. D **60**, 2126–2132 (2004). doi:10.1107/S0907444904019158
20. B.W. Matthews, Solvent content of protein crystals. J. Mol. Biol. **33**, 491–497 (1968). doi:10.1016/0022-2836(68)90205-2
21. S.B. Singh, H. Jayasuriya, K.B. Herath et al., Isolation, enzyme-bound structure, and activity of platensimycin A1, from *Streptomyces platensis*. Bioorg. Med. Chem. Lett. **40**, 4756–4759 (2009). doi:10.1016/j.tetlet.2009.06.118